STELLAR EVOLUTION. VII. THE EVOLUTION OF A 2.25 $M_\odot$ STAR FROM THE MAIN SEQUENCE TO THE HELIUM-BURNING PHASE*

ICKO IBEN, JR.
Massachusetts Institute of Technology, Cambridge, Massachusetts
Received June 27, 1966

ABSTRACT

Prior to reaching the giant phase, the evolution of a 2.25 $M_\odot$ star is qualitatively identical with the evolution of more massive stars examined in earlier papers of this series. After reaching the giant branch, 2.25 $M_\odot$ evolution is quite similar to that of lighter stars examined earlier. The 2.25 $M_\odot$ star is very near the limiting mass above which helium flashing will not occur. Near the top of the red-giant branch, nuclear burning via the $N^{14} \rightarrow O^{18}$ reactions is initiated in an electron-degenerate core. The ensuing development of the "N^{14}-flash" phase is followed until the star begins to descend from the red-giant tip

I. INTRODUCTION

In Paper II of this series (Iben 1965*b*), it was conjectured that the rise along the red-giant branch of a low-mass population I star is permanently halted with the initiation of the $N^{14}(\alpha,\gamma)F^{18}(\beta^+\nu)O^{18}$ reactions in the stellar core. In the present paper, preliminary work toward a verification of this conjecture is presented. A 2.25 $M_\odot$ star is evolved well into the phase of "N^{14} flashing," until the star begins the descent from the red-giant tip. Considerable work is yet required to determine whether core degeneracy will be lifted and central temperatures drop prior to ignition of the triple-alpha process or whether the period of the "N^{14} flash" will merge smoothly into the "helium-flash" phase.

A star of mass 2.25 $M_\odot$ has been chosen for several reasons. In stars with a mass in excess of 3 $M_\odot$, helium burning in the stellar core is initiated under non-degenerate conditions. In stars with a mass below 1.5 $M_\odot$ (Paper VI, Iben 1967), core degeneracy becomes considerable along the giant branch prior to the initiation of helium burning. An examination of 2.25 $M_\odot$ evolution is thus a step in the direction of determining the critical mass above which the helium-flash phenomenon does not occur. In Paper VI it was indicated that (using the standard relaxation technique) the computation time involved in following a low-mass star up the giant branch becomes almost prohibitively long. On the other hand, higher-mass stars are followed readily from the main-sequence through core helium-burning phases. A choice of mass as close as possible to the critical mass for helium flashing is therefore, from an economic standpoint, highly desirable.

II. OVER-ALL CHARACTERISTICS PRIOR TO CORE HELIUM BURNING

To emphasize the similarities and the differences between the observable properties of stars which exhibit the helium-flash phenomenon and stars which do not, paths in the H-R diagram for both the 2.25 $M_\odot$ star and the 3 $M_\odot$ star described in Paper II are juxtaposed in Figure 1. Times to reach numbered points along the paths are given in Table 1 in units of 10^8 yr. The critical mass for helium flashing lies somewhere between 2.25 $M_\odot$ and 3 $M_\odot$.

The qualitative features of evolution prior to reaching the giant branch (points 1 to 10) are identical in the two cases. Differences along the red-giant branch are due to the fact that electrons become degenerate in the hydrogen-exhausted core of the 2.25 $M_\odot$ star. Helium burning by the $N^{14}(\alpha,\gamma)F^{18}(\beta^+\nu)O^{18}$ reactions begins at point 11 along the

* Supported in part by the National Aeronautics and Space Administration (NSG-496).

3 $M_\odot$ track and reverses the upward rise only temporarily. The 3 $M_\odot$ star rises again, from point 12 to 13, until the $3\alpha \rightarrow C^{12}$ reactions permanently halt further upward motion. At a given luminosity along the two giant branches, temperatures in the electron-degenerate core of the 2.25 $M_\odot$ star are lower than in the core of the 3 $M_\odot$ star. Hence the 2.25 $M_\odot$ star is more luminous than the 3 $M_\odot$ star when the $N^{14} \rightarrow O^{18}$ reactions are ignited in the core. If, as expected, the evolution upward of the 2.25 $N_\odot$ star is halted permanently by the $N^{14} \rightarrow O^{18}$ reactions at point 13, then the 2.25 $M_\odot$ red-giant tip will be a magnitude more luminous than the 3 $M_\odot$ red-giant tip. If the $N^{14} \rightarrow O^{18}$ reactions are neglected or if core degeneracy is effectively lifted in the 2.25 $M_\odot$ star before N^{14} is exhausted near the stellar center, then the 2.25 $M_\odot$ star will rise eventually almost 2.5 mag further before the $3\alpha \rightarrow C^{12}$ reactions assume a dominant role in the stellar core.

The time dependence of interior and observable characteristics of the 2.25 $M_\odot$ star is shown in Figures 2 and 3. These figures are to be compared with Figures 2 and 3 in Paper II (3 $M_\odot$) and with Figures 6 and 7 in Paper VI (1.5 $M_\odot$). It is evident that,

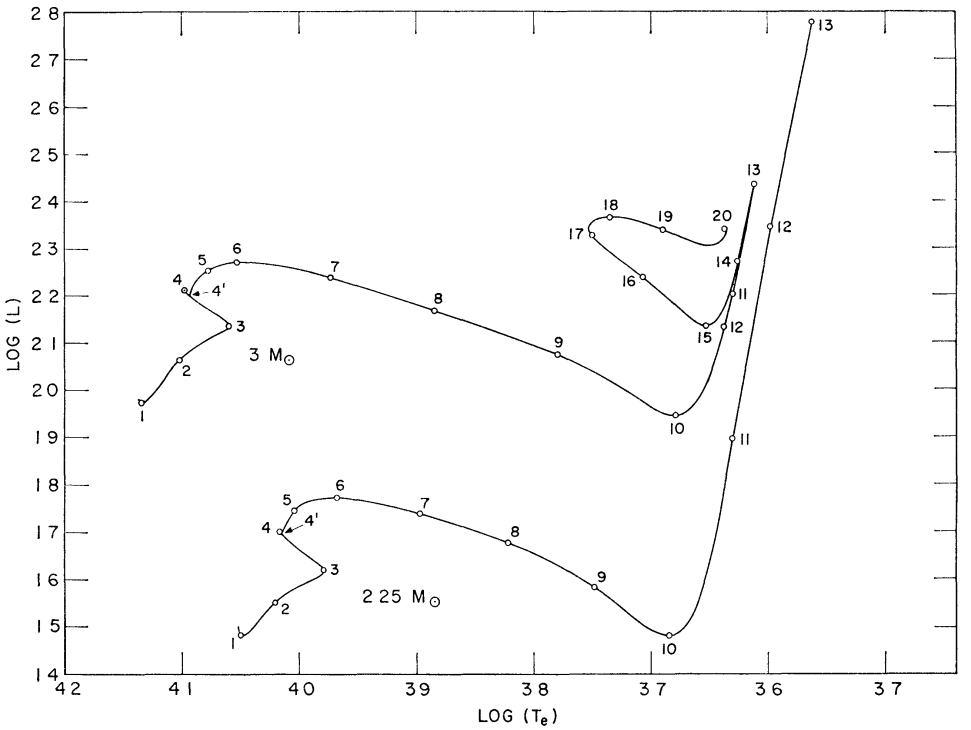

FIG. 1.—The evolutionary paths of population I stars of mass 2.25 $M_\odot$ and 3 $M_\odot$. Times to reach labeled points along each track are given in Table 1. Luminosity is in solar units and surface temperature is in degrees Kelvin.

TABLE 1

EVOLUTIONARY LIFETIMES (10^8 YR)

Point	2 25 $M_\odot$	3 $M_\odot$	Point	2 25 $M_\odot$	3 $M_\odot$	Point	2 25 $M_\odot$	3 $M_\odot$
1	0 058550	0 024586	5	5 2017959	2 40119	10	5 5157054	2 48925
2	2 7988965	1 38921	6	5 3846801	2 44420	11	5 6167250	2 49817
3	4 8502987	2 23669	7	5 4459513	2 47004	12	5 7773918	2 50728
4	5 0150323	2 34089	8	5 4736797	2 47865	13	5 8986139	2 53163
4′	5 0173994	2 34222	9	5 4947244	2 48429			

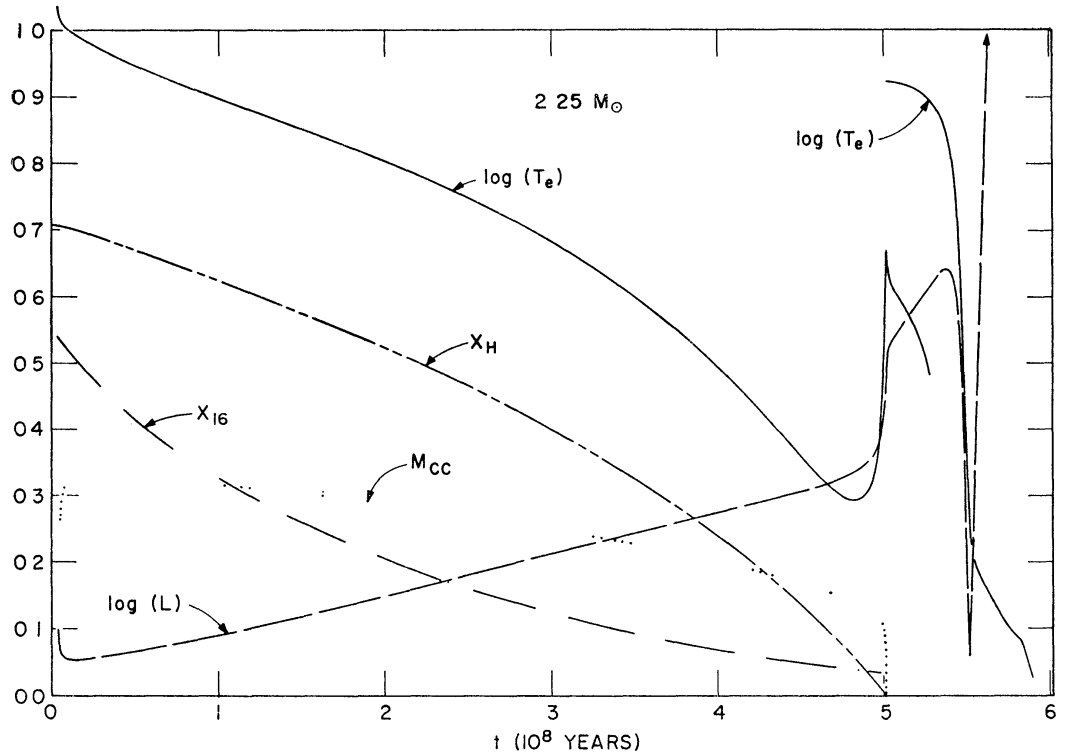

FIG. 2 —The variation with time of luminosity (L), surface temperature (T_e), mass fraction in the convective core (M_{CC}), and central abundances by mass of $H^1(X_H)$ and $O^{16}(X_{16})$. Time (t) in this figure and in Figs. 3 and 8 is measured in units of 10^8 yr. The unit of luminosity is $L\odot = 3.86 \times 10^{33}$ ergs/sec and the unit of surface temperature is degrees Kelvin. Scale limits correspond to $1.45 \leq \log L \leq 1.95$, $3\ 95 \leq \log T_e \leq 4\ 05$ ($t \leq 5\ 26$), $3\ 55 \leq \log T_e \leq 4\ 05$ ($t \geq 5.01$), $0\ 0 \leq M_{CC} \leq 0\ 445$, $0.0 \leq X_H \leq 1\ 0$, and $0\ 0 \leq X_{16} \leq 0\ 02$.

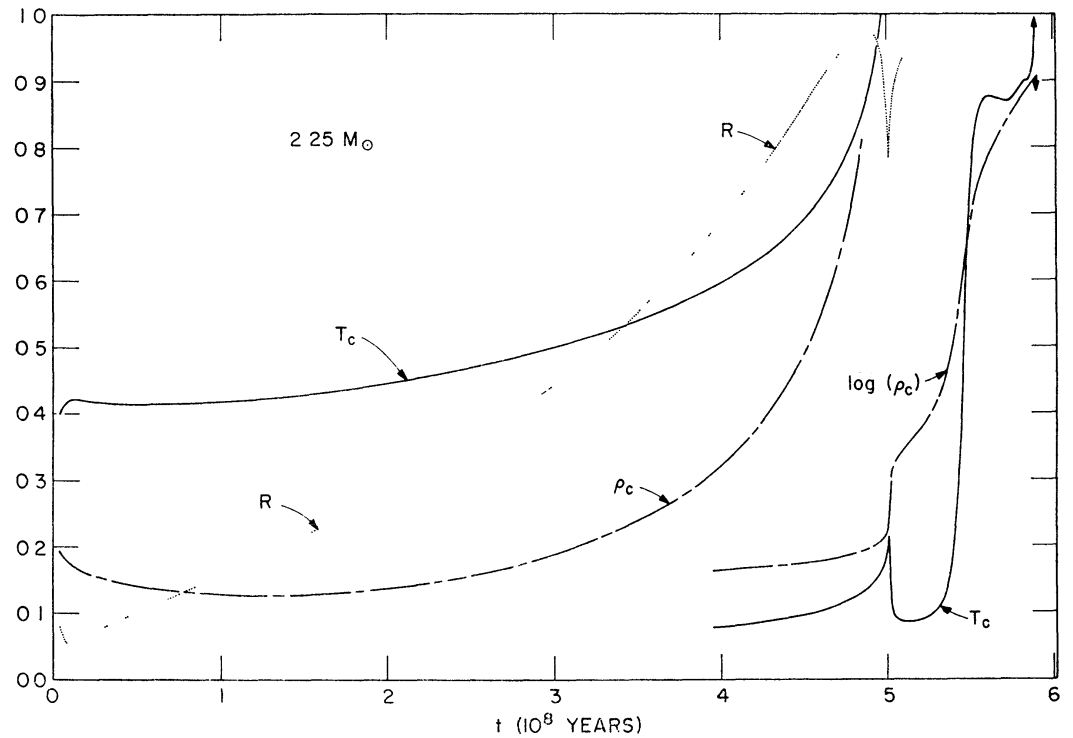

FIG. 3.—The variation with time of central temperature (T_c), central density (ρ_c), and radius (R). Units are $10^{6\circ}$ K for temperature, grams per cubic centimeter for density, and $R\odot = 6.96 \times 10^{10}$ cm for radius. Scale limits correspond to $18 \leq T_c \leq 28$ ($t \leq 4\ 96$), $20 \leq T_c \leq 70$ ($t \geq 3.94$), $50 \leq \rho_c \leq 100$, $1 \leq \log \rho_c \leq 6$, and $1.4 \leq R \leq 2.4$.

before the base of the red-giant branch is reached, 2.25 $M_\odot$ characteristics depend on time in a fashion qualitatively identical with those of more massive stars. After the base of the giant branch is reached, 2.25 $M_\odot$ behavior is more closely akin to the behavior of less massive stars. In particular, the temperature at the center of the 2.25 $M_\odot$ star drops briefly, along the giant branch, as electron degeneracy begins to contribute dominantly to core pressures.

III. STRUCTURAL DETAILS PRIOR TO THE GIANT PHASE

To provide an opportunity for a more complete comparison with stars described in earlier papers, structural details during several characteristic phases of 2.25 $M_\odot$ evolution will be briefly presented.

The distribution of characteristics within the 2.25 $M_\odot$ star at $t = 4.39 \times 10^6$ yr, shortly before the main sequence is reached, is given in Figure 4. Within the convective core, whose boundary is marked by the discontinuity in the He^3 abundance, energy is produced primarily by the CN cycle reactions. Energy production between the edge of the convective core and mass fraction 0.30 is contributed predominantly by the reactions which convert C^{12} into N^{14}. Beyond mass fraction 0.30, the major contribution to escaping energy is the release of gravitational energy from the still-contracting envelope. Within the convective core, C^{12} has been converted almost entirely into N^{14} and the center of the C^{12} transition layer occurs at a mass fraction 0.196.

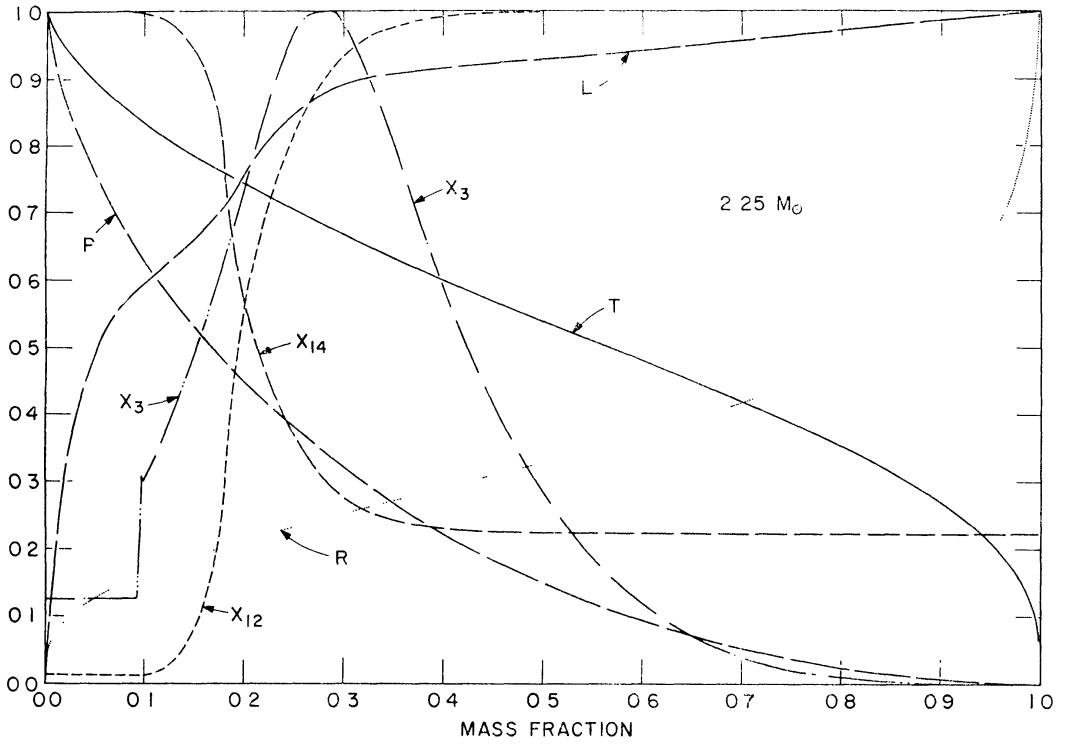

FIG. 4.—The variation with mass fraction of state and composition variables when $t = 4\ 3880680 \times 10^6$ yr. Variables in this figure and in Figs 5–7 have the significance: ρ = density (gm/cm^3), T = temperature ($10^{6\circ}$ K), P = pressure (10^{17} dynes/cm^2), L = luminosity ($3\ 86 \times 10^{33}$ ergs/sec), R = radius (6.96×10^{10} cm), and central abundance by mass of $H^1(X_H)$, $He^3(X_3)$, $C^{12}(X_{12})$, and $N^{14}(X_{14})$. Scale limits correspond to $0.0 \leq \rho \leq 59\ 914$, $0\ 0 \leq T \leq 21.967$, $0\ 0 \leq P \leq 1.7856$, $0\ 0 \leq L \leq 32.291$, $0.0 \leq R \leq 1.1443$, $0.0 \leq X_{14} \leq 5\ 40 \times 10^{-3}$, $0\ 0 \leq X_{12} \leq 3\ 61 \times 10^{-3}$, and $0.0 \leq X_3 \leq 3.59 \times 10^{-5}$. The mass fraction in the static envelope is 1.144065×10^{-3} as it is in Figs 5–7, and stellar radius is $R_s = 1.48515\ R_\odot$.

Conditions within the star at $t = 3.31 \times 10^8$ yr, when the central hydrogen abundance has been reduced to about one-half of its initial value, are shown in Figure 5. Nuclear-energy sources are highly concentrated toward the center, and 95 per cent of the total nuclear-energy production occurs within the convective core. The center of the C^{12} transition layer occurs at a mass fraction 0.433, and He^3 has reached a maximum abundance by mass, $(X_3)_{max} = 6.09 \times 10^{-4}$, at a mass fraction 0.595.

At $t = 5.09 \times 10^8$ yr, conditions within the star are as shown in Figure 6. The star has just embarked on the period of hydrogen burning in a thick shell. In comparison with more massive stars, this period is relatively extended since, as seen from Figure 6,

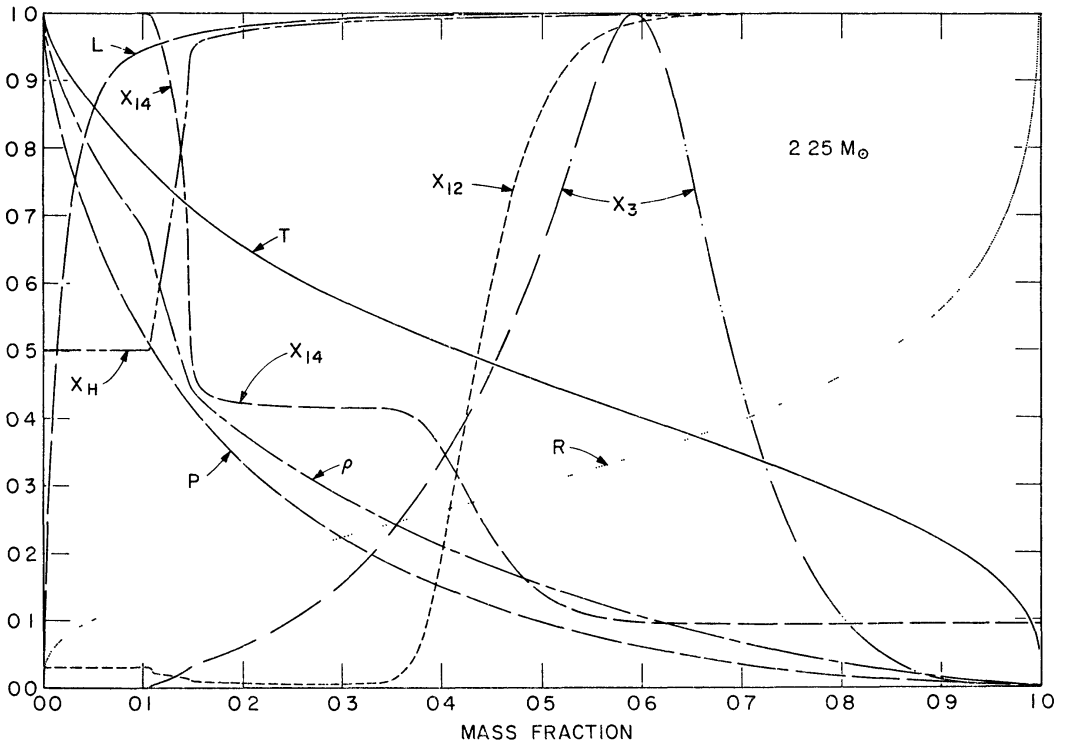

FIG. 5.—The variation with mass fraction of state and composition variables when $t = 3\ 3097994 \times 10^8$ yr. Variables have the same significance and units as in Fig 4 Scale limits correspond to $0.0 \leq \rho \leq 60.796$, $0\ 0 \leq T \leq 23\ 216$, $0\ 0 \leq P \leq 1.397$, $0.0 \leq L \leq 36\ 788$, $0\ 0 \leq R \leq 1\ 4526$, $0\ 0 \leq X_H \leq 0.708$, $0.0 \leq X_3 \leq 6\ 09 \times 10^{-4}$, $0.0 \leq X_{12} \leq 3\ 61 \times 10^{-3}$, and $0\ 0 \leq X_{14} \leq 1.30 \times 10^{-2}$. Stellar radius is $R_s = 1.9078\ R_\odot$.

hydrogen is effectively exhausted over only the inner 5 per cent of the star's mass at the start of the phase. Within the nearly isothermal, hydrogen-exhausted core, approximately 94 per cent of the original O^{16} has been converted into N^{14}. The center of the C^{12} transition layer still occurs at mass fraction 0.433 and the maximum abundance of He^3, which has risen to $(X_3)_{max} = 7.16 \times 10^{-4}$, still occurs at mass fraction 0.595. Li^7 has been destroyed over the inner 98.66 per cent of the star's mass.

The center of the hydrogen-burning shell ($L = 0.5\ L_{surface}$) is located at mass fraction 0.0850 and shell thickness is $\Delta M_{sh}/M_{star} = 0.0524$. At the shell center, temperature $T_{sh} = 23.0 \times 10^6$ ° K, density $\rho_{sh} = 79$ gm/cm^3, and the hydrogen abundance is $X_H = 0.155$.

In Figure 7 are shown interior conditions at $t = 5.51 \times 10^8$ yr, just before the star reaches the base of the red-giant branch. The hydrogen-burning shell is centered at mass fraction 0.11107 and shell thickness is $\Delta M_{sh}/M_{star} = 4.748 \times 10^{-3}$. Temperature,

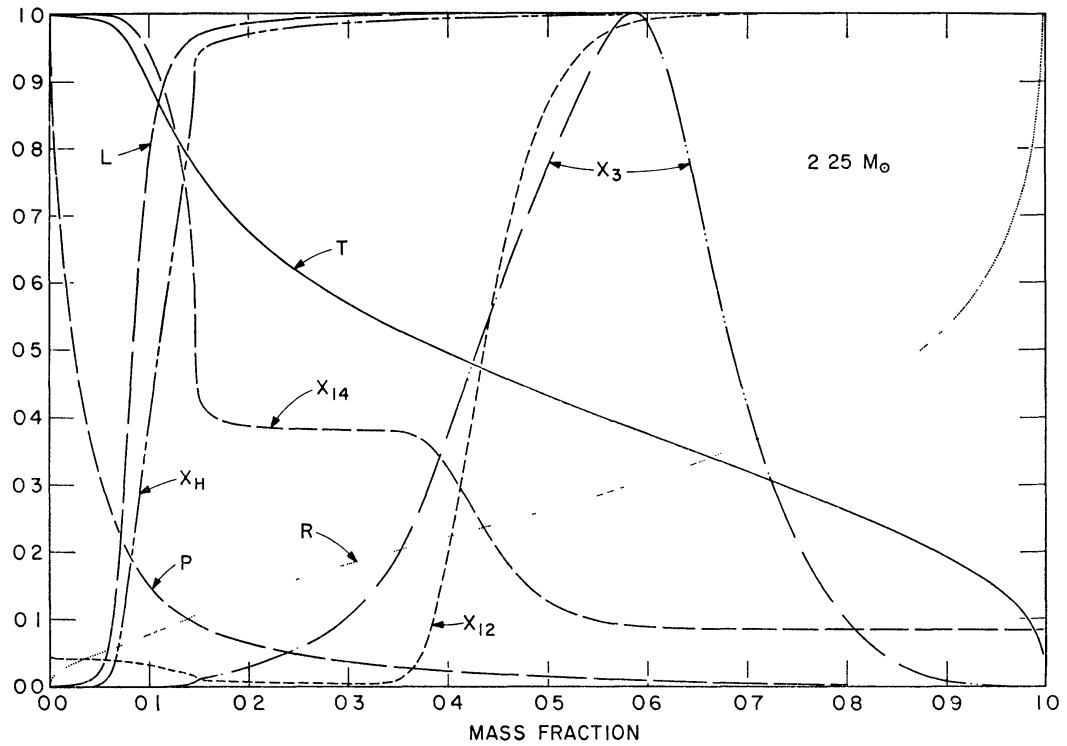

FIG. 6 —The variation with mass fraction of state and composition variables when $t = 5\ 0887085 \times 10^8$ yr Scale limits correspond to $0\ 0 \leq \rho \leq 509.60$, $0.0 \leq T \leq 24\ 341$, $0.0 \leq P \leq 7.8869$, $0.0 \leq L \leq 53\ 002$, $0\ 0 \leq R \leq 1\ 7366$, $0\ 0 \leq X_H \leq 0\ 708$, $0.0 \leq X_3 \leq 7\ 16 \times 10^{-4}$, $0.0 \leq X_{12} \leq 3.61 \times 10^{-3}$, and $0\ 0 \leq X_{14} \leq 0\ 0142$. Stellar radius is $R_s = 2\ 3267\ R\odot$.

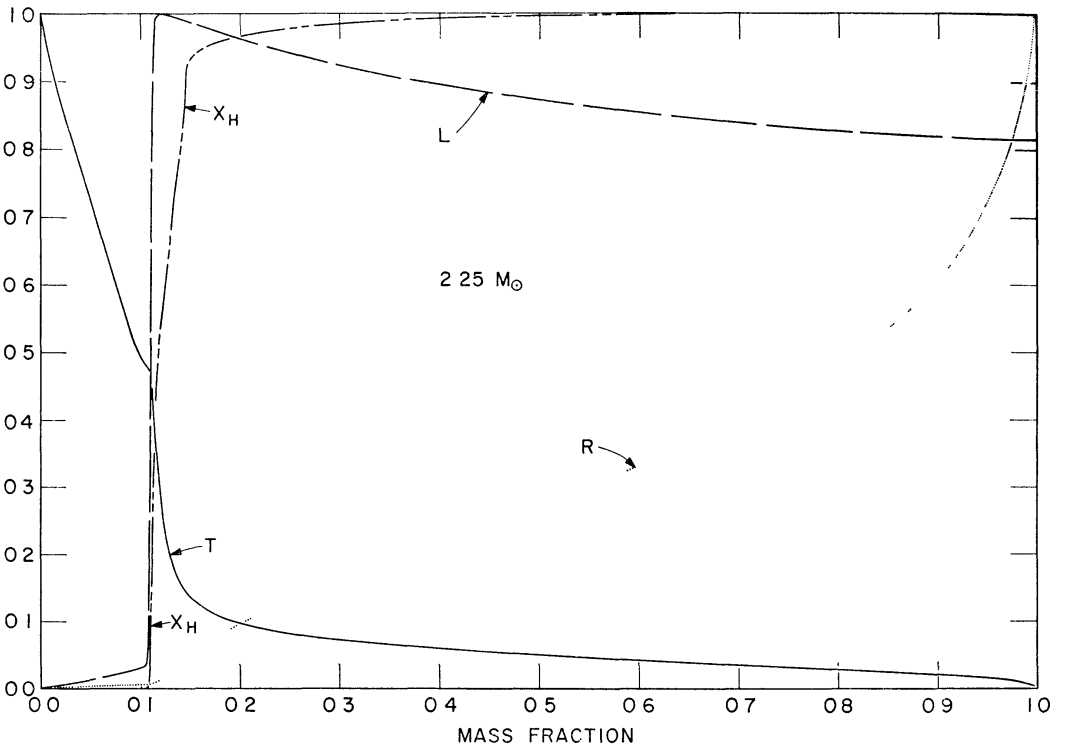

FIG. 7.—State and composition variables as a function of mass fraction when $t = 5.5090646 \times 10^8$ yr. Scale limits correspond to $0\ 0 \leq \rho \leq 32034$, $0\ 0 \leq T \leq 56\ 977$, $0\ 0 \leq P \leq 1698\ 3$, $0.0 \leq L \leq 38.271$, $0\ 0 \leq R \leq 6.7407$, $0\ 0 \leq X_H \leq 0\ 708$, $0.0 \leq X_3 \leq 7.31 \times 10^{-4}$, $0.0 \leq X_{12} \leq 3\ 61 \times 10^{-3}$, and $0\ 0 \leq X_{14} \leq 0\ 0142$. Stellar radius is $R_s = 7.3597\ R\odot$.

density, and hydrogen abundance at the shell center are $T_{sh} = 26.2 \times 10^6$ ° K, $\rho_{sh} = 155$ gm/cm^3, and $X_H = 0.079$.

At the stellar center, where $T_c = 56.98 \times 10^6$ ° K and $\rho_c = 32034$ gm/cm^3, electron degeneracy accounts for roughly one-third of the total pressure.

The time dependence of a few characteristics during the shell-narrowing phase is shown on an expanded scale in the left-hand portion of Figure 8 (see below). Shell "base" has been defined arbitrarily as the point at which the abundance of hydrogen has been reduced to $X_H = 0.01$. As before, shell center is defined as the point at which the

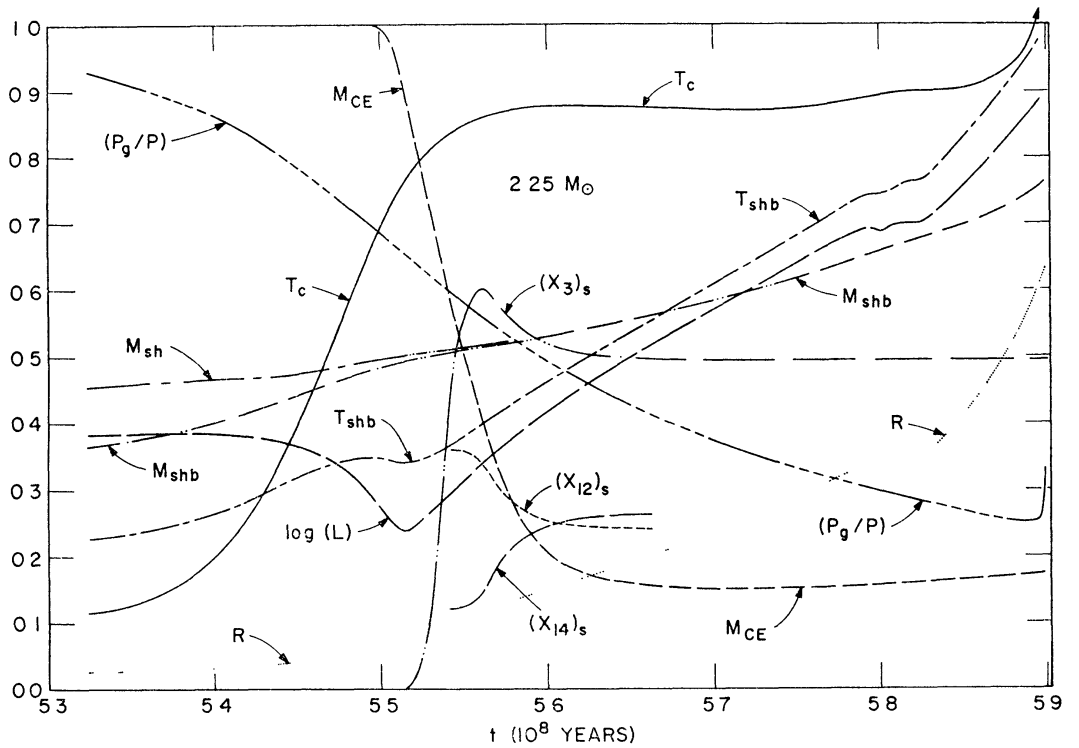

FIG. 8 —The variation with time t (10^8 yr) of central temperature (T_c), stellar radius (R), surface luminosity (L), mass fraction outside of which energy is carried by convection (M_{CE}), mass fraction at the shell center (M_{sh}), mass fraction at the "base" of the shell where $X_H = 0\ 01$ (M_{shb}), temperature at the base of the shell (T_{shb}), ratio of pressure computed in the perfect-gas approximation to total pressure at the center (P_g/P), and surface abundances by mass of $N^{14}(X_{14})$, $C^{12}(X_{12})$, and $He^3(X_3)$. Luminosity and radius are in solar units and temperatures are in units of 10^6 ° K. Scale limits correspond to $20 \leq T_c \leq 70$, $0 \leq R \leq 100$, $1 \leq \log L \leq 3$, $0 \leq M_{CE} \leq 1$, $0 \leq M_{sh}$, $M_{shb} \leq \frac{2}{3}$, $20 \leq T_{shb} \leq 40$, $0 \leq (X_{14})_s, (X_{12})_s \leq 0\ 01$, and $0\ 0 \leq (X_3)_s \leq 5 \times 10^{-4}$.

luminosity variable is at half-maximum. At the start of the shell-narrowing phase, the shell "base" is at mass fraction 0.0867 and the shell center is at mass fraction 0.103. At the base of the red-giant branch, shell "base" and shell center are, respectively, at mass fraction 0.1098 and 0.1116. Note that electron degeneracy at the center, as measured by P_g/P, is significant during the entire shell-narrowing phase. Between $t \sim 5.385 \times 10^8$ yr and $t \sim 5.516 \times 10^8$ yr, the contribution of electron degeneracy to total pressure at the center rises from 12 to 35 per cent.

IV. EVOLUTION ALONG THE GIANT BRANCH

As the star approaches the base of the red-giant branch, energy flow by convection occurs over a rapidly increasing region extending downward from the surface (see curve M_{CE} versus t in Fig. 8). As a result of mixing, the surface Li^7 abundance begins to drop

according to the rule $(Li^7)_s = (Li^7)_s^0 \times (0.0134)/\Delta M_{CE}$), where ΔM_{CE} is the mass fraction in the convective envelope and $(Li^7)_s^0$ is the surface Li^7 abundance as the star reaches the main sequence. As the star begins its ascent along the giant branch, and convection extends into the region where considerable He^3 has been formed during the main-sequence phase, the surface He^3 abundance begins to increase; see curve $(X_3)_s$ in Figure 8. The surface He^3 abundance reaches a maximum of $(X_3)_s \cong 3.02 \times 10^{-4}$ when the lower boundary of the convective envelope reaches the point where He^3 achieved its maximum abundance during the main-sequence phase. As convection extends deeper yet, surface He^3 drops. The decline continues at a modest rate until the base of the convective envelope begins to recede outward in mass fraction. Then, $(X_3)_{surface} = 2.47 \times 10^{-4}$. Surface abundances of C^{12} and N^{14} begin to change (see curves $(X_{12})_s$ and $(X_{14})_s$ in Fig. 8) when the base of the convective envelope reaches the C^{12} transition layer below which C^{12} has been converted almost completely into N^{14} during the main-sequence phase. Final surface abundances are $(X_{12})_s = 2.4 \times 10^{-3}$ and $(X_{14})_s = 2.64 \times 10^{-3}$. The surface ratio of N^{14} to C^{12} thus increases from an initial value of $\frac{1}{3}$ to 1.1.

Just as in more massive stars, core temperatures in the 2.25 $M_\odot$ star rise extremely rapidly during the shell-narrowing phase (see T_c versus t in Fig. 8). However, just as in the lighter stars studied in Paper VI, the rate of increase of core temperatures is inhibited by the increasing importance of electron degeneracy. When electron degeneracy accounts for roughly one half of the total central pressure, central temperature begins to drop. The value of central temperature, $T_c = 63.8 \times 10^6$ ° K, when this occurs is about twice as high as the central temperatures in the lower-mass stars examined in Paper VI. Since, at central densities of (1–4) $\times 10^5$ gm/cm^3 the $N^{14}(\alpha,\gamma)F^{18}(\beta^+\nu)O^{18}$ reactions begin to exert a significant influence when T_c reaches 66–67 $\times 10^6$ ° K, it is clear that the mass 2.25 $M_\odot$ is almost equal to the critical mass above which helium flashing does not occur. It must be emphasized that this conclusion would be altered if the chosen effective cross-section for the $N^{14}(\alpha,\gamma)F^{18}$ reaction were grossly in error.

As the star ascends further and further along the giant branch, the hydrogen-exhausted core becomes more and more closely isothermal. This may be seen from curves T_c and T_{shb} in Figure 8. Central temperature changes very slowly, but shell temperatures rise steadily.

The rates at which shell temperatures, stellar luminosity, and stellar radius increase with time change abruptly at $t = 5.795 \times 10^8$ yr and again at $t = 5.823 \times 10^8$ yr. The first abrupt change occurs at the shell passes through the mass fraction reached by the convective core at its maximum extent during the core hydrogen-burning phase. The second abrupt change occurs as the shell passes through the mass fraction reached by the convective envelope at its maximum extent during the giant phase. Thus both changes occur when the shell encounters a region where the dependence of composition variables on mass fraction changes abruptly.

It is of interest that the base of the convective envelope recedes toward the surface (in mass fraction) as it is approached by the hydrogen-burning shell (see curves M_{CE} and M_{shb} in Fig. 8). This is comforting, from the point of view of simplicity, but hardly surprising, since convection will certainly not extend inward beyond the base of the shell.

Throughout the giant phase, the thickness of the hydrogen-burning shell decreases steadily in mass fraction. The minuteness which the shell can achieve is exhibited in Figure 9, where several variables in the vicinity of the shell are plotted versus mass fraction for times $t_1 = 5.862949 \times 10^8$ yr and $t_2 = 5.863825 \times 10^8$ yr. In both cases, shell thickness is $\Delta M_{sh}/M_{star} \cong 1.662 \times 10^{-4}$. Thirteen relaxation time steps separate the two models. Since the shell center has moved through a mass fraction of $\sim 2.22 \times 10^{-4}$, or $\sim 1.71 \times 10^{-5}$ per time step, approximately ten time steps are required for the shell to move through a mass fraction equal to its thickness. It has been found by experience that, for a given time interval, a minimum in the quantity—number of time steps multiplied by number of iterations per time step—is achieved when time steps are chosen

such that the shell moves through one-tenth of its thickness per step. An algorithm has been devised to speed up the calculation of red-giant evolution; this algorithm is described in the Appendix. It has been applied successfully to carry the 2.25 $M_\odot$ star to the start of the helium-burning phase.

V. THE EARLY DEVELOPMENT OF THE "N^{14} FLASH"

As pointed out in the previous section, the temperature gradient in the hydrogen-exhausted core becomes progressively less steep during a major portion of the ascent along the red-giant branch. This is illustrated more clearly by the temperature profiles in Figure 10, curves 1–4. Central temperature remains roughly constant while temperatures in the neighborhood of the shell rise steadily.

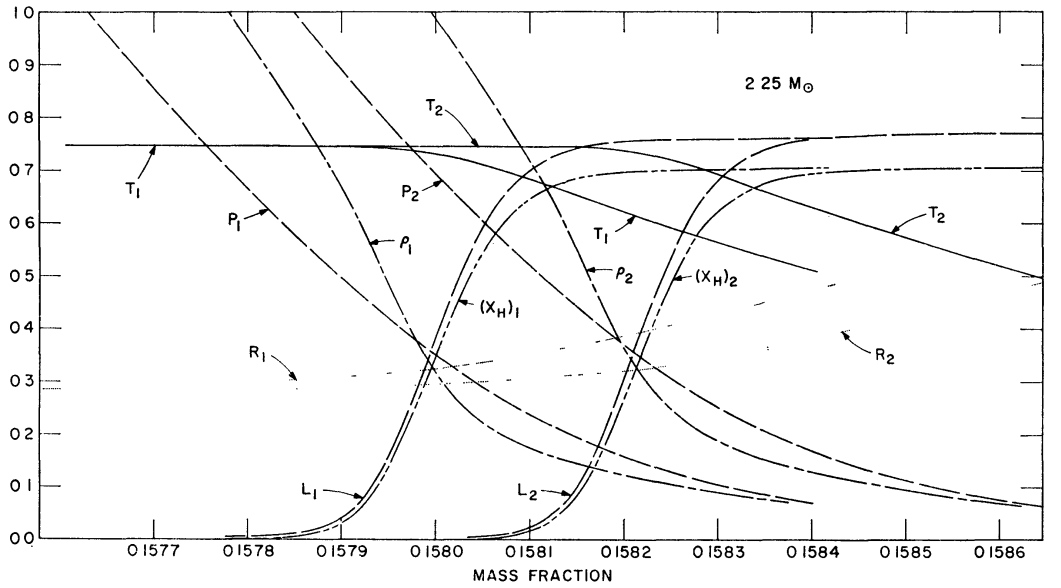

FIG. 9.—The variation with mass fraction of quantities near the shell when $t = t_1 = 5.8629494 \times 10^8$ yr and $t_2 = 5.8638250 \times 10^8$ yr. Luminosity and radius are in solar units. Pressure, temperature, and density are in units of 10^{17} dynes/cm^2, 10^6 ° K, and gm/cm^3, respectively. Scale limits correspond to $0 \leq L \leq 500$, $0.0 \leq R \leq 0.1$, $0 \leq P \leq 5$, $0 \leq T \leq 50$, $0 \leq \rho \leq 150$, and $0 \leq X_H \leq 1$.

Eventually, central temperatures do rise enough that nuclear burning by the $N^{14} \rightarrow O^{18}$ reactions begins to affect the behavior of physical variables near the center. The influence of core nuclear burning becomes noticeable when the central temperature reaches about 66×10^6 ° K. The content of Table 2 summarizes the subsequent development.

In model 1, the rate ϵ_{nuc} at which nuclear energy is released *at* the center has become equal to the rate ϵ_g at which gravitational and thermal energy is released *from* the center. In model 2, all of the energy released at the center from the gravitational field is used up in increasing the thermal energy of particles near the center. Thereafter, a portion of the nuclear energy released goes also into raising the thermal-energy content of matter near the center. In model 3, a convective core has just begun to form. In model 4, the central density has reached a maximum and the matter near the center starts to expand. In addition to supplying energy for increased thermal motions near the center, nuclear sources now also supply the energy required for expansion. In model 5, the expansion of central regions has finally begun to affect observable characteristics by inhibiting the rate at which temperatures and densities rise in the hydrogen-burning shell. After model 5, stellar luminosity decreases and the star begins its descent from the red-giant tip. In model 6, core temperatures are rising extremely rapidly and the degree of electron

degeneracy in the core is, correspondingly, being rapidly reduced. The star has entered well into the "N^{14}-flash" phase.

A most interesting feature of the flash phenomenon is that observable characteristics of the star are affected only indirectly: none of the nuclear energy released in the core reaches the surface. This is illustrated in Figure 11 by luminosity profiles near the center, shortly after the convective core has formed. Essentially all of the nuclear energy released near the center is absorbed within the convective core. That a good portion of the nuclear energy released goes into increasing the thermal-energy content of the core is illustrated by the temperature profiles (curves 5–8) in Figure 10. The boundary of the convective core is marked by the near-discontinuity in the temperature gradient at mass fraction less than 0.05.

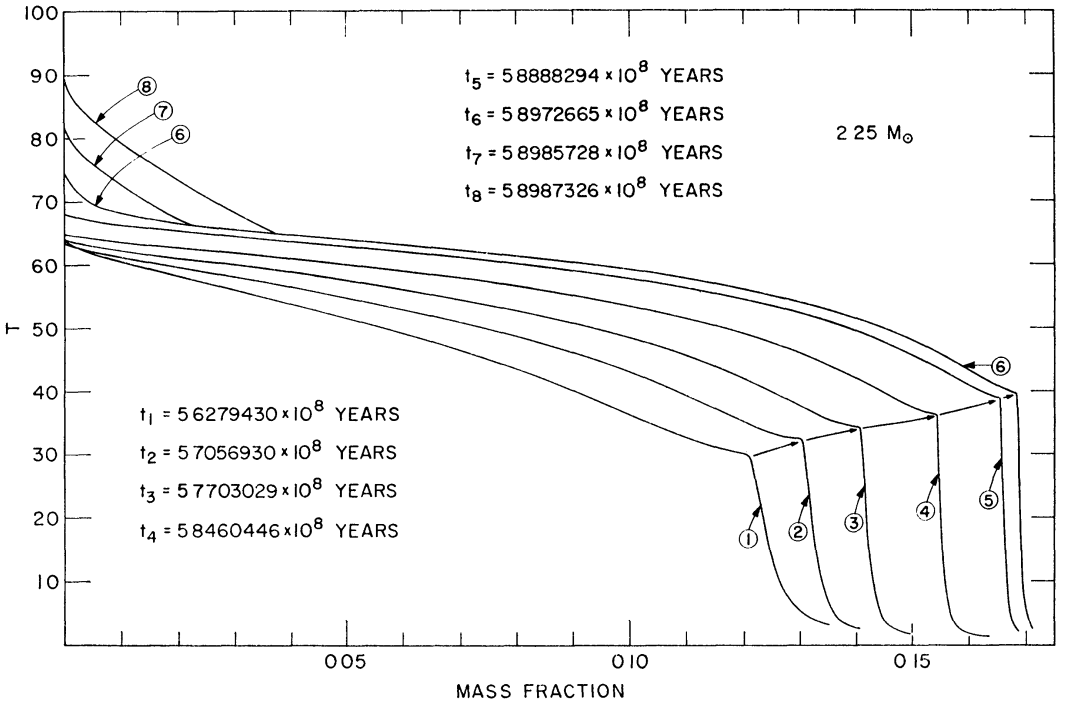

FIG. 10 —Temperature versus mass fraction for several times along the giant branch $0 \leq T \leq 10^{8.0}$ K.

TABLE 2

MODEL CHARACTERISTICS DURING THE N^{14} FLASH

Model	Model Description	Time*	Δt†	T_c‡	ρ_c§	(ϵ_{nuc})‖	L_s#	R_s**
1.	$(\epsilon_{nuc}=\epsilon_g)_c$	5 8708241	. . . .	66 084	298824	1 51	419 51	48 580
2	$(\epsilon_g)_c=0$	5 8862025	153 784	67 778	320930	4 54	516 63	55 723
3	$M_{CC}>0$	5 8959402	97 377	71 815	335762	16 2	596 81	61 230
4	ρ_{max}	5 8977614	18 212	75 857	336945	192	613 54	62 442
5.	L_{max}	5 8986139	8 525	82 427	332350	3560	618 43	63 155
6	Last model	5 8987348	1 209	92 503	320904	115000	616 39	62 988

* 10^8 yr
† Time interval between successive models (10^4 yr)
‡ Central temperature ($10^{6.0}$ K)
§ Central density (gm/cm³)
‖ Energy-generation rate at center (erg gm^{-1} sec^{-1})
Surface luminosity ($L_\odot$)
** Stellar radius ($R_\odot$)

The distribution of several characteristics within the last model computed is shown in Figure 12. The degree of electron degeneracy is constant throughout the convective core, the boundary of which occurs at a mass fraction 0.0463. Electron degeneracy accounts for approximately two-thirds of the total pressure at every point within the core. This is to be compared with the start of the flash phase when electron degeneracy accounts for about three-fourths of the total pressure at the center. Nuclear energy is being released in the core via the $N^{14} \rightarrow O^{18}$ reactions at the rate $L_{nuc} = 280\ L_\odot$. None of this energy escapes from the core. The hydrogen-burning shell is centered at a mass fraction 0.16923 and has a thickness $\Delta M_{sh}/M_{star} = 1.357 \times 10^{-4}$. Temperature and density at the shell center are $T_{sh} \sim 38.88 \times 10^6$ ° K and $\rho_{sh} \sim 38$ gm/cm^3.

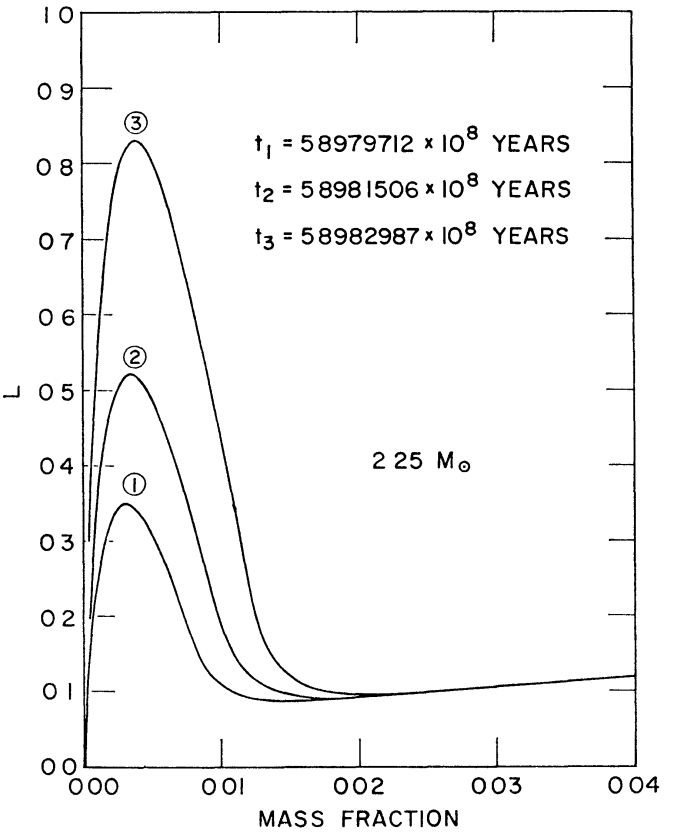

FIG. 11 —Luminosity versus mass fraction for several times near the beginning of the N^{14} flash. $0 \leq L \leq L_\odot$.

The abundance by mass of N^{14} in the core of the last model is $X_{14} = 0.0129$. Throughout the period of N^{14} burning in a convective core, the core N^{14} abundance has remained essentially constant at this value. As much N^{14} is added to the core by mixing from regions just outside the growing core as is burned near the center. There has thus been no diminution in the fuel supply in central regions where rapid burning takes place.

It is difficult to anticipate the results of further evolution. During the early portion of the star's rise along the giant branch, electron degeneracy stops the increase of central temperature when it accounts for approximately half of the central pressure. One might therefore expect a change in the character of the flash development when electron degeneracy is reduced until it again accounts for only half of the central pressure. On the basis of the temperature profiles in Figures 10 and 12, we might extrapolate that this situation will occur when central temperature approaches 120×10^6 ° K. If, prior to

this time, the $N^{14} \rightarrow O^{18}$ reactions have occurred rapidly enough to cause N^{14} to vanish in the core, core temperatures will be sufficiently high to sustain helium burning by the triple-alpha process. The star will settle down to a relatively quiet phase of helium burning in a non-degenerate core and point 13 in Figure 1 represents the red-giant tip of the 2.25 $M_\odot$ star.

If N^{14} has not been scoured out by the time degeneracy has been effectively lifted, the higher rate of the $N^{14} \rightarrow O^{18}$ reactions will force the star to pass through a phase of N^{14} burning in a non-degenerate core wherein temperatures are too low for significant helium burning by the triple-alpha process. After N^{14} has been exhausted near the center, the stellar core will again become degenerate and the star will rise again along the 2.25 $M_\odot$ giant branch beyond point 13 in Figure 1.

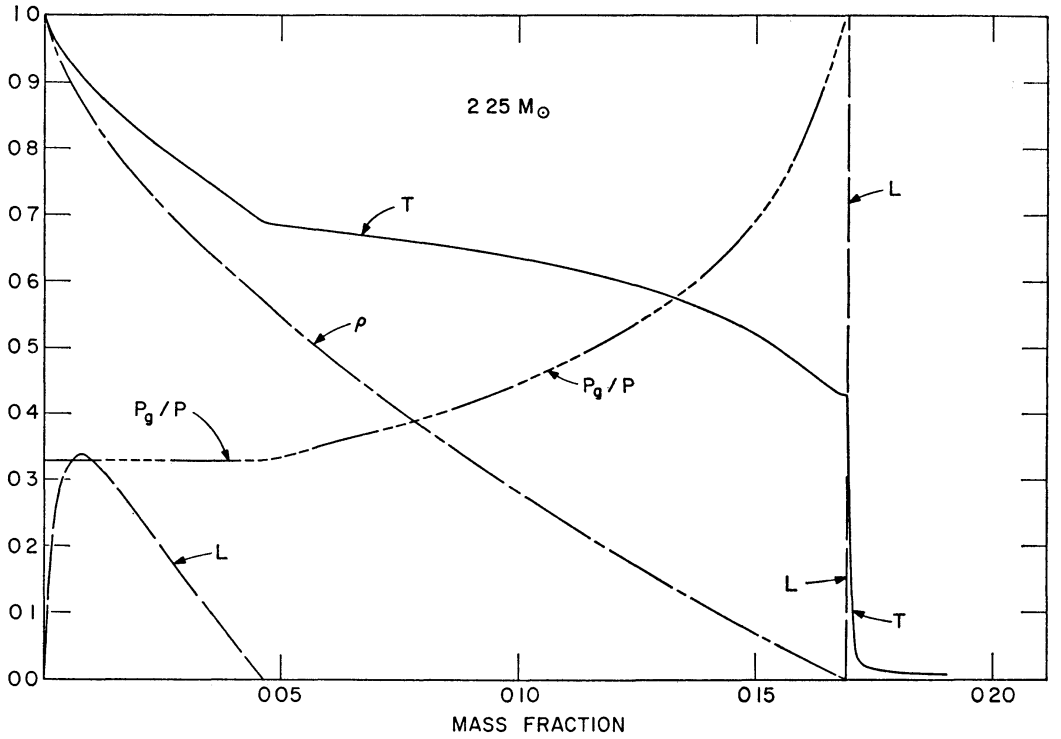

FIG. 12 —Interior characteristics when $t = 5.8987348 \times 10^8$ yr. Scale limits correspond to $0.0 \leq$ temperature $(T) \leq 92.503 \times 10^6$ ° K, $0\,0 \leq$ density $(\rho) \leq 3.2090 \times 10^5$ gm/cm³, $0\,0 \leq$ pressure in the perfect-gas approximation divided by total pressure $(P_g/P) \leq 1.0$, and $0.0 \leq$ luminosity $(L) \leq 616\,39\,L_\odot$.

In the event that the latter evolution occurs, it is pertinent to estimate the luminosity at the red-giant tip defined by the ignition of the triple-alpha process. This estimate will also pertain to the situation when the $N^{14} \rightarrow O^{18}$ reactions are neglected entirely. Earlier it was indicated that the energy release by the $N^{14} \rightarrow O^{18}$ reactions begins to affect interior behavior significantly when central temperature approaches $T_c = 66 \times 10^6$ °K. Then $\epsilon_{nuc} = 1.5$ ergs/gm/sec. At a density of $\sim(3\text{–}4) \times 10^5$ gm/cm³, the triple-alpha process will supply energy at a comparable rate when the central temperature approaches $T_c \sim 75\text{–}76 \times 10^6$ ° K. From Figure 8 one finds that when $T_c \sim 66 \times 10^6$ ° K, $d\ (\log L)/dT_c \sim 0.116/10^6$ ° K. Thus, in the event that the $N^{14} \rightarrow O^{18}$ reactions are absent, the 2.25 $M_\odot$ star will rise by $\Delta(\log L) \sim 1.1$ beyond point 13 in Figure 1 before evolution upward along the giant branch is finally halted. The red-giant tip will therefore be 2.5 mag brighter than if the $N^{14} \rightarrow O^{18}$ reactions permanently halt the upward rise.

Thanks are due to the Laboratory for Nuclear Science at the Massachusetts Institute of Technology for the use of its IBM 7044 computer. The Center for Space Research at the Massachusetts Institute of Technology has been most generous in supplying financial support.

APPENDIX

AN ALGORITHM FOR RED GIANTS

Using the relaxation technique described in Appendix A of Paper I (Iben 1965*a*), the minimum computational time required to achieve a given change in observable and interior stellar characteristics along the red-giant branch is limited by the minuteness of the hydrogen-burning shell and the concomitant near-discontinuity in all physical variables in the vicinity of this shell. The optimum time-step size (to achieve, for a given time interval, a minimum in the product: number of iterations per step $\times$ number of steps) corresponds to an increase per step in the mass of the hydrogen-exhausted core equal to approximately 10 per cent of the thickness of the shell (defined as the mass interval within which 80 per cent of the nuclear-energy generation occurs). The thickness of the shell diminishes to $\sim(10^{-3}$–$10^{-4})M_{\odot}$ along the giant branch and central temperatures do not reach values high enough for significant helium burning until the core mass reaches values on the order of 0.4 $M_{\odot}$. Hence, in order to reach core helium-burning stages by a persistent use of the standard relaxation technique, from $\sim 4 \times 10^3$ to 4×10^4 steps are required. With computation times of $\sim$1–2 minutes per step, this means that several hundred hours of computation time may be necessary.

In order to minimize computational effort, an algorithm has been devised which can reduce computational times by at least a factor of 10 without sacrificing the aim of achieving a fairly reliable time-dependent sequence of models. This algorithm is motivated by the observation that the shell "wave form" (= the distribution versus mass of all physical variables in the vicinity of the shell) changes almost imperceptibly with each small-scale time step and may be treated as a near-invariant over the course of many small-scale time steps.

The procedure consists of alternating large-scale projections with small-scale relaxation time steps. To begin the algorithm, suppose that two models separated by many small-scale relaxation steps are available. Let these models be called 1 and 2. For the purpose of standardization, let the shell center in each model be defined as the position at which the abundance by mass of hydrogen is exactly one half of the surface hydrogen abundance. Let M_{s1} and M_{s2} denote the masses corresponding to the shell center in models 1 and 2, respectively. Finally, let the "shell vicinity" be defined for model 2 as the region bounded by masses M_A and M_B such that

$$M_A = M_{s2}(1 - \delta_A) \leq M \leq M_{s2}(1 + \delta_B) = M_B ,$$

where δ_A and δ_B are chosen at discretion and varied with experience.

For masses M_{i2} in model 2 such that $M_{s2} \leq M_{i2} \leq M_B$, define related masses in model 1 by

$$M_{i1} = M_{i2} - (M_B - M_{i2})\frac{M_{s2} - M_{s1}}{M_B - M_{s2}} = M_{i2} - (\delta M_i)_B$$

and related masses in the projected model 3 by

$$M_{i3} = M_{i2} + (\delta M_i)_B \times f,$$

where f may be set as desired, subject to restrictions yet to be described.

For masses in model 2 such that $M_A \leq M_{i2} \leq M_{s2}$, define related masses in model 1 and in the projected model 3 by

$$M_{i1} = M_{i2} - (M_{i2} - M_A)\frac{M_{s2} - M_{s1}}{M_{s2} - M_A} = M_{i2} - (\delta M_i)_A ,$$

$$M_{i3} = M_{i2} + (\delta M_i)_A \times f .$$

For masses in model 2 such that $M_{i2} < M_A$ or $M_{i2} > M_B$, define related masses in models 1 and 3 by $M_{i1} = M_{i2} = M_{i3}$.

By logarithmic interpolation, the quantities $Q_{i1}(k)$ $(= P, T, L, R)$ appropriate to the masses M_{i1} are found and the variables $Q_{i3}(k)$ appropriate to the masses M_{i3} in the projected model are determined by

$$\ln Q_{i3}(k) = \ln Q_{i2}(k) + [\ln Q_{i2}(k) - \ln Q_{i1}(k)] \times f .$$

The magnitude of f is limited by the requirement that pressure decreases and radius increases monotonically outward in the projected model.

The time Δt_{23} elapsed between the projected model 3 and model 2 is approximated by the relation

$$\Delta t_{23} = \Delta t_{12} \frac{L_{1H} + L_{2H}}{L_{2H} + L_{3H}} f ,$$

where Δt_{12} is the time elapsed between models 1 and 2 and L_{1H}, L_{2H}, and L_{3H} are the rates at which energy is being liberated in the three models by hydrogen-burning reactions. This choice for Δt_{23} is based on the assumption that the total energy emitted by the hydrogen-burning shell is related to the increase in mass of the hydrogen-exhausted core by a factor which is independent of time. Since the CN cycle is the dominant mode whereby hydrogen is converted into helium along the giant branch, this assumption is justified to a high degree of accuracy.

Between the core boundary ($X_H = 0$) and the convective envelope (which begins just outside of the shell) composition parameters at masses M_{i3} in model 3 are assumed to be identical with composition parameters at the corresponding masses M_{i2} in model 2. Within the core and within the convective envelope, the changes in composition parameters are computed in the normal fashion (see Appendix A in Paper I) with the time step Δt_{23} and with the temperature and density distributions in models 2 and 3.

After the complete model 3 has been obtained, a small-scale relaxation step is instituted to obtain a final model 3′. The values of all physical variables in the first trial model for 3′ are obtained from the values of these same variables in model 3, using the changes $\sigma_i(k)$ (defined in Appendix A of Paper I) appropriate to the last small-scale step which led to model 2. Mass shells in the first trial model for 3′ are altered and composition changes throughout the star are computed in the manner described in Paper I. Iterations then proceed until difference equations appropriate to each mass shell are satisfied to the desired accuracy.

Model 2 now becomes model 1 and model 3′ becomes model 2. Another large-scale projection followed by a small-scale relaxation step leads to a new model 3′. This procedure may be continued indefinitely, with f chosen in such a way that large-projection time steps Δt_{23} are always equal to the initial Δt_{23}. From time to time, however, it is advisable to begin afresh with a long sequence of small-scale relaxation steps not interrupted by large-scale projections. In this way the distribution of composition and state variables will be restored to a more faithful representation of the star than would be the case if large- and small-scale steps were alternated indefinitely. For example, shell thickness decreases during evolution up the giant branch, whereas a large-scale projection tends to maintain shell thickness constant.

REFERENCES

Iben, Icko, Jr. 1965*a*, *Ap. J.*, **141**, 993 (Paper I).
———. 1965*b*, *ibid.*, **142**, 1447 (Paper II).
———. 1967, *ibid.*, **147**, 624 (Paper VI).